Scattering of hydrogen ions and atoms in gases

V. I. Radchenko and G. D. Ved'manov

Ural State Technical University, 620000 Ekaterinburg, Russia
(Submitted 18 May 1994; resubmitted 31 August 1994)
Zh. Eksp. Teor. Fiz. **107**, 3–19 (January 1995)

Scattering of H^+ and H^- ions and $H^0(1s)$ atoms in gases, with or without their charge being altered, has been studied both experimentally and theoretically. We describe the experimental setup and a method of reducing the errors in measuring the charge distributions $\Phi_i(t)$. Cross sections $\sigma_{\bar{1}0}$, $\sigma_{\bar{1}1}$, and σ_{01} have been measured at energies $E=1.67$, 5.0, 6.9, 10.4, and 14.9 MeV, as have the efficiencies $\Phi_0^{\max}$ with which the H^- ions are neutralized, together with the target thicknesses $t^{\max}$, which characterize the interaction of H^- and $H^0(1s)$ particles with the He, Ar, Kr, Xe, H_2, O_2, CO_2, and C_2H_2 gases. The Born approximation for an H_2 target in the $E=0.1$–20 MeV energy range has been used to calculate scattering cross sections and characteristic scattering angles for hydrogen particles in collisions of type $(\bar{1}0)+(\bar{1}1)$, (00), $(\bar{1}\bar{1})$, and (11). A molecular hydrogen target is described using the Wang, Weinbaum, and Stewart form factors. We analyze these results, and compare them with one another and with the results of other researchers. © *1995 American Institute of Physics.*

1. INTRODUCTION

Progress in ion–atom collision physics is related primarily in a natural way to the study of the interaction of light particles, such as H^+ and H^- ions and H^0 atoms, with gaseous targets. From a practical standpoint, this is due to a need for devices producing high-power beams of hydrogen ions and atoms with small angular divergence and emittance to heat the plasma in fusion reactors, to transport particle beams over large distances, and for use in storage rings, colliding-beam accelerators, etc. It also results from a need to predict the effect of the medium in which the beams propagate on the beams themselves. From a theoretical standpoint, light particles serve as the most convenient testing ground for building and verifying numerical models of various processes.

Despite the historically rather long period of development of this field of ion–atom collision physics, there have been neither systematic nor experimental studies of the cross sections for electron loss or capture by hydrogen particles with energies E higher than 1 MeV in interactions with heavy atomic and molecular gases. This is even more true of scattering that leaves the original charge on the incoming particles unaltered, of the angular characteristics of all the aforementioned processes, of scattering in polarized vapor targets, etc. For one thing, almost everything just said (except for data on the electron loss cross sections) holds for an H_2 target. The most complete and successful theoretical studies have involved only atomic hydrogen and helium targets,[1–9] while experimental work relates to H_2 and He.[1–4,10–17]

From 1982 to 1986 we carried out a series of experiments to measure the cross sections and characteristic scattering angles of hydrogen particles emerging as a result of the loss of one or two electrons by H^- ions and $H^0(1s)$ atoms with energies E ranging from 1–15 MeV in gases, the scattering cross section of H^+, H^0, and H^- particles when their original charge is unaltered, and the production cross section of hydrogen atoms in the $2s$ and $2p$ states in the neutralization of H^- ions. Later these processes were studied theoretically. With Refs. 11 and 12 we started publication of the physical part of the completed theoretical and experimental studies, while some topics pertaining to the measurement method are reflected in Refs. 18–20. The first paper[11] gives measurements of the scattering cross sections σ_{ii} for H^+, H^0, and H^- particles with charge unaltered and the cross sections and characteristic angles for the $(\bar{1}\bar{1})$, (00), (11), and $(\bar{1}0)+(\bar{1}1)$ processes in which fast hydrogen particles interact with a helium target. The second paper[12] contains experimental data on the cross sections $\sigma_{\bar{1}0}$, $\sigma_{\bar{1}1}$, and σ_{01} for H^- and $H^0(1s)$ particles with energies $E=1.67$ and 5.0 MeV; it also contains Born-approximation calculations of cross sections and characteristic scattering angles for H^-, H^0, and H^+ particles with energies E in the 0.1–20 MeV range for $(\bar{1}0)+(\bar{1}1)$ processes and collisions that leave the charge of atomic hydrogen unaltered, and, within the derived instantaneous dipole moment approximation, in targets consisting of atoms of alkali metals and molecules of alkali-halide compounds.

In the present paper we examine, in the Born approximation, electron loss by H^- ions and the scattering of the hydrogen particles H^+, $H^0(1s)$, and H^- with incident-particle energies E in the 0.1–20 MeV range in collisions with a molecular-hydrogen target. In experiments at $E=1.67$, 5.0, 6.9, 10.4, and 14.9 MeV, we have determined the cross sections $\sigma_{\bar{1}0}$, $\sigma_{\bar{1}1}$, and σ_{01} for the loss of one or two electrons by H^- ions and $H^0(1s)$ atoms in interactions with He, Ar, Kr, Xe, H_2, O_2, CO_2 and C_2H_2 gases, and we have measured both the efficiency $\Phi_0^{\max}$ with which H^- ions are neutralized and the corresponding target thicknesses $t^{\max}$.[12] The experimental results for $E=6.9$, 10.4, and 14.9 MeV are published for the first time; the data for $E=1.67$ and 5.0 MeV were obtained by the authors of the present paper, and are presented here to complete the background required for analysis of the experimental data.

 1063-7761/95/010001-09$10.00

2. EXPERIMENTAL SYSTEM AND RESULTS OF MEASUREMENTS

The experimental system consists of standard detection and monitoring electronics, plus vacuum, gas, and other devices commonly used to measure the charge distribution of particles in beams (i.e., the fraction $\Phi_i(t)$ of particles with charge i in the beam after traversing a target of thickness t). The H^- ions are accelerated in a conventional U-120 cyclotron and then, via a beam-bending magnet, directed into the test channel.[11] A distinctive feature of the apparatus is the high degree of beam collimation and, as a result, the possibility of maintaining a particle flux after traversing the gas collision chamber at a level J less than 500 particles per second, which makes it possible to detect the charge distribution of the hydrogen particles H^+, H^0, and H^- using a set of three surface-barrier silicon detectors (typeDKPs-350) operating in the direct particle-counting mode, thus yielding low noise and interference. The particle flux in a definite charge state is measured by processing the detector signals in a spectrometric circuit consisting of a charge-sensitive preamplifier, a pulse-shaper, a differential amplitude discriminator, and a counter. With allowance for the pulsed mode of operation of the accelerator at the average intensity J mentioned above, errors resulting from the superposition of electrical signals in the apparatus did not exceed 0.5%.

A detailed description of the main components of the experimental apparatus and the measurement of the charge composition of the beam of fast hydrogen particles is given in Refs. 11, 12, and 20. Here we touch only on problems encountered in reducing the cross-section measurement errors.

One of the main sources of error is related to determining the effective thickness t of the gas target. Cross sections were measured at a gas pressure P in the collision chamber (in the range 0.1–1 Pa[11,12]) which, on the one hand, was a compromise between a decreasing error in gas pressure measurements (as the pressure increased) and an increasing uncertainty in the size of the additional target formed by the gas flowing out of the collision chamber and, on the other, minimized the random error in determining $\Phi_i(t)$. The net error in measuring t was at most 5–7%.

Numerical analysis of Eqs. (4)–(6) in Ref. 12 for calculating σ_{01}, $\sigma_{\bar{1}0}$, and $\sigma_{\bar{1}1}$ shows that the magnitude of the error in measuring the cross sections depends to a large extent on the stability, and hence the "purity," of the original charge makeup of the beam, $\Phi_i(t=0)$, at the entrance to the collision chamber filled with the gas being studied. This is also especially important for the (01) process, because the presence in the original beam of atoms in long-lived excited states (specifically in the metastable $2s_{1/2}$ state)—in addition to the $H^0(1s)$ atoms—can result in an erroneous overestimate of the measured cross sections σ_{01}, since the cross sections for electron loss by excited $H^0(nl)$ atoms are considerably higher than the cross section for electron loss by the ground state of the hydrogen atom (see, e.g., Ref. 5). In view of this, the $H^0(1s)$ beam was prepared using a charge-exchange gas target[11] equipped with a differential vacuum pump system, and an electric deflector to separate the beam into charge fractions and destroy long-lived states of $H^0(nl)$ atoms. The pump was also used to maintain a high vacuum at a level of less than 10^{-4}Pa, and there was also a way to apply a magnetic field to a section (0.40 m long) that the beam passed through before entering the collision chamber. This guaranteed destruction of the excited $H^0(nl)$ states and "cleared" the beam of extraneous charge fractions. The same was done with the original beam of H^+ and H^- ions. As a result, the original charge distribution of particles at the entrance to the collision chamber was almost the same at all energy values E, and was maintained at $\Phi_{\bar{1}}(0)=0.988$ and $\Phi_0(0)=0.010$ for the original H^- beam and at $\Phi_0(0)=0.995$ for the original $H^0(1s)$ beam.

The charge distribution of the particles in the beam must be preserved after it leaves the collision chamber only over the section that the beam traverses from the collision chamber to the system that separates the beam into different charge components. This was accomplished by implementing differential pumping immediately after the collision chamber (this was partly done before the collision chamber, although there was really no need to do so, because the entrance slit of the collision chamber, which is needed to collimate the beam and restrict the gas flow, has extremely small dimensions, $0.02\times 6\text{mm}^2$, while the exit slit is $0.3\times 6\text{mm}^2$) in order to maintain a high vacuum in this section (residual gas pressure $<3\cdot 10^4$Pa), and by placing the separating electric and magnetic deflectors as close as possible to the collision chamber ($\cong 0.2$ m for the electric deflector and $\cong 1.2$ m for the magnetic deflector).[11,12,20]

Note that using semiconductor detectors to detect the charged components of the beams, rather than measuring devices of other types, on the whole helped reduce the errors in measuring the fractions $\Phi_i(t)$. No errors in measuring $\Phi_i(t)$ due to possible defects in the sensitive surfaces of the detectors (in reference measurements in which the beam was moved in relation to the detectors) were detected at the statistical-error level.

Our experimental estimates, calculations of the differential scattering cross sections for particles in the $(\bar{1}0)$ process carried out in Refs. 8,11 and 12, and conclusions drawn in Refs. 7, 12 and 17 about the weak dependence of the characteristic scattering angles on the type of gas target have shown that the acceptance of the detectors was always much greater than the emittance of some one of the charged components of the beam.

Figure 1 depicts the experimental dependence of the charged fraction of the beam, $\Phi_i(t)$, on the thickness of a C_2H_2 target for an initial beam of H^- ions with energy $E=5.0$ MeV. $\Phi_i(t)$ is observed to behave in just the same way with other targets and collision energies.

Table I lists the cross sections calculated from the measured charge distributions, the H^- ion neutralization efficiencies $\Phi_0^{\max}$ observed at target thicknesses $t^{\max}$, and the values δ of random experimental errors corresponding to the same standard deviation. With experimental errors taken into account, these values obey the following basic rules:

1. At fixed incident particle energy, the electron-loss cross sections form the sequence $\sigma_{\bar{1}0}>\sigma_{01}>\sigma_{\bar{1}1}$ and increase with the atomic number of monatomic gases and with

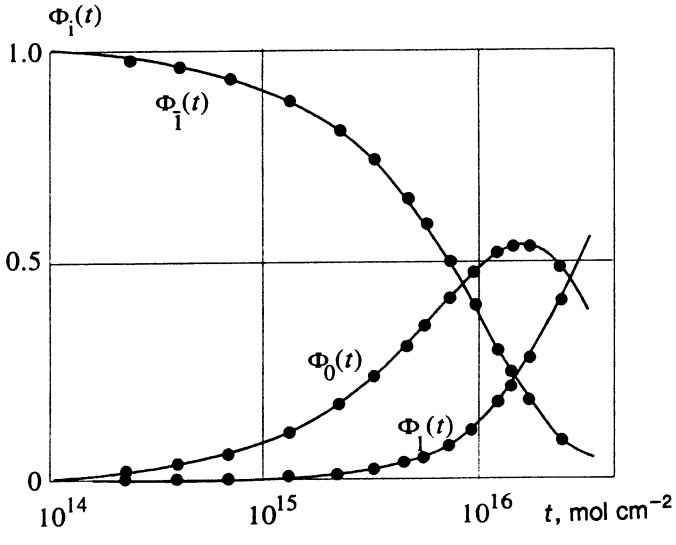

FIG. 1. A typical pattern of the measured charge distribution of hydrogen particles as a function of the thickness of the C_2H_2 target for an initial H^- ion beam with energy $E=5.0$ MeV.

the atomic numbers of the particles comprising molecular targets (approximately in accordance with the additivity law[12]).

2. For a single target, the cross sections $\sigma_{\bar{1}0}$, σ_{01}, and $\sigma_{\bar{1}1}$ decrease (with increasing energy) according to a universal functional dependence $\sim E^{-n}$, as a result of which the efficiency Φ_0^{max} with which H^- ions are neutralized in the target is independent of the collision energy. For all targets, $n\leqslant 1$.

3. The thickness t^{max} at which the value Φ_0^{max} is reached is proportional to E^n and increases as heavy targets are replaced with lighter targets at fixed energy E.

3. CALCULATION OF CROSS SECTIONS FOR AN H_2 TARGET

We consider the following processes in which fast hydrogen particles interact with a molecular-hydrogen target:

$$H^+ + H_2 \rightarrow H^+ + H_2(\Sigma), \tag{1}$$

$$H^0(1s) + H_2 \rightarrow H^0(1s,2s,2p_0) + H_2(\Sigma), \tag{2}$$

$$H^- + H_2 \rightarrow H^-(1s^2) + H_2(\Sigma), \tag{3}$$

$$H^- + H_2 \rightarrow H^0(nl) + H_2(\Sigma) + e^-, \tag{4}$$

$$H^- + H_2 \rightarrow H^+ + H_2(\Sigma) + 2e^-, \tag{5}$$

in which we take into account all final states of the target, both from the discrete spectrum and the continuous, which is denoted by the symbol Σ.

Our starting point is the general perturbation-theory formula for the differential cross section in the center-of-mass frame of reference obtained in the first Born approximation without relativistic corrections:[21]

TABLE I. Experimental data on the cross sections σ_{01}, $\sigma_{\bar{1}0}$, and $\sigma_{\bar{1}1}$ (in units of 10^{-18}cm^2) and the neutralization efficiencies Φ_0^{max} for H^- ions observed at gaseous target thicknesses t^{max} (in units of 10^{15}cm^{-2}).

Gas	E,MeV	σ_{01}	$\sigma_{\bar{1}0}$	$\sigma_{\bar{1}1}$	Φ_0^{max}	t^{max}
	1.67	8.62	29.7	1.20	0.543	63.2
	5.0	4.61	10.9	0.190	0.526[c]	136[c]
He	6.9	2.68	7.82	0.135	0.557	170
	10.4	1.62	4.96	0.0620	0.576[c]	332[c]
	14.9	1.22	3.88	0.0643	0.553	487
	1.67	117	319	19.2	0.518	4.95
	5.0	60.4	125	4.62	0.495[c]	11.0[c]
Ar	6.9	44.4	106	3.77	0.511	12.9
	10.4	30.8	80.1	1.93	0.519	16.6
	14.9	25.2	61.2	1.67	0.532	20.9
	1.67	135	328	22.5	0.511	4.60
	5.0	66.5	165	8.19	0.524[c]	8.99[c]
Kr	6.9	68.5	157	6.70	0.511	8.62
	10.4	49.9	124	4.05	0.531[c]	12.1[c]
	14.9	43.8	108	3.37	0.517	12.2
	1.67	170	403	33.9	0.504	2.98
	5.0	105	229	12.0	0.500[c]	6.10[c]
Xe	6.9	96.4	225	7.64	0.519	6.76
	10.4	74.4	185	8.09	0.527[c]	8.04[c]
	14.9	65.1	160	5.67	0.509	8.79
	1.67	11.8	42.7	1.24	0.582	40.8
	5.0	4.70	15.3	0.287	0.581	117
H_2	6.9	3.63	11.4	0.409	0.592	125
	10.4	2.38	8.18	0.172	0.576	231
	14.9	1.71	5.37	0.159	0.580	346
	1.67	106	274	15.3	0.518	5.80
	5.0	44.0	110	4.01	0.528	13.4
0_2	6.9	32.7	86.9	2.62	0.528	18.5
	10.4	22.3	59.8	1.32	0.525	22.1
	14.9	16.7	47.5	2.63	0.534	31.4
	1.67	131	331	17.4	0.528	4.78
	5.0	58.2	145	4.56	0.530	10.0
CO_2	6.9	42.7	110	3.22	0.536	13.5
	10.4	27.5	77.3	2.06	0.531	19.9
	14.9	21.7	61.3	1.58	0.547	25.2
	1.67				0.548	
	5.0	32.8	89.3	2.05	0.544	15.1
C_2H_2	6.9				0.550	22.0
	10.4				0.548	32.0
	14.9				0.546	71.7
δ,%	1	7	9	25	1	12

The superscript "c" indicates that the corresponding values of Φ_0^{max} and t^{max} were not measured directly but calculated using Eq. (7) of Ref. 12 from the measured cross sections, and δ is the measurement error.

$$\frac{d\sigma_{\alpha_f\beta_f}(\nu)}{do} = \frac{M^2}{4\pi^2\hbar^4}\frac{k_f}{k_i}\left|\int\int Ue^{-i\mathbf{qR}}\Psi_f^*\Psi_i d\mathbf{R}d\tau\right|^2, \tag{6}$$

where α_f and β_f stand for the final states of the incident and scattered particles, respectively; ν is the scattering angle in the center-of-mass frame; M is the reduced mass of the colliding systems; $\mathbf{k}_i$ and $\mathbf{k}_f$ are the wave vectors corresponding to the motion of a particle with reduced mass M and the velocity of the incident particle before and after the collision; $\mathbf{q}=\mathbf{k}_f-\mathbf{k}_i$; U is the potential energy of the interaction of the

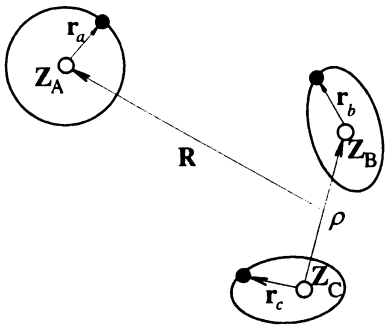

FIG. 2. Diagrammatic illustration of the notation used in specifying the coordinates of the particles participating in a collision of system A with a diatomic molecule BC.

particles; **R** is the distance between the centers of mass of the particles; and $d\tau$ is an element of the configuration space of the electrons of both particles. For a scattering process A+BC→... in which a monatomic particle A is scattered by a diatomic molecule BC and in which electron exchange processes are ignored, the initial and final wave functions in Eq. (6) can be written as

$$\Psi_i = \psi_{\alpha_i}(\mathbf{r}_a)\psi_{\beta_i}(\mathbf{r}_b,\mathbf{r}_c), \quad \Psi_f = \psi_{\alpha_f}(\mathbf{r}_a)\psi_{\beta_f}(\mathbf{r}_b,\mathbf{r}_c), \tag{7}$$

where ψ_{α_i} and ψ_{α_f}, and ψ_{β_i} and ψ_{β_f} are the wave functions, respectively, of the initial and final states of particles A and BC; $\mathbf{r}_a$ is the radius vector of the ath electron of particle A with respect to its nucleus; $\mathbf{r}_b$ and $\mathbf{r}_c$ are the radius vectors of the bth and cth electrons with respect to the nuclei of B and C in the molecule. It is convenient at this point to assign to the nucleus of B the same number of molecular electrons (more precisely, with allowance for exchange processes, the radius vectors of those electrons), including outer electrons, as belong to particle B, and to assign the remaining electrons to the nucleus of C, which is reflected in the notation of the arguments of the molecule's wave function in (7) and in the expression for U below Eq. (8). This notation is illustrated by Fig. 2.

Let $\boldsymbol{\rho}$ be the internuclear distance vector in the BC molecule. Then the potential energy of the interaction of the colliding systems is

$$\begin{aligned} U = e^2\Bigg\{ & \frac{Z_A Z_B}{|\mathbf{R}-\boldsymbol{\rho}/2|} + \frac{Z_A Z_C}{|\mathbf{R}+\boldsymbol{\rho}/2|} - Z_A\sum_{b=1}^{N_B}\frac{1}{|\mathbf{R}-\boldsymbol{\rho}/2-\mathbf{r}_b|} \\ & - Z_A\sum_{c=1}^{N_C}\frac{1}{|\mathbf{R}+\boldsymbol{\rho}/2-\mathbf{r}_c|} - Z_B\sum_{a=1}^{N_A}\frac{1}{|\mathbf{R}-\boldsymbol{\rho}/2+\mathbf{r}_a|} \\ & - Z_C\sum_{a=1}^{N_A}\frac{1}{|\mathbf{R}+\boldsymbol{\rho}/2+\mathbf{r}_a|} + \sum_{a=1}^{N_A}\sum_{b=1}^{N_B}\frac{1}{|\mathbf{R}-\boldsymbol{\rho}/2+\mathbf{r}_a-\mathbf{r}_b|} \\ & + \sum_{a=1}^{N_A}\sum_{c=1}^{N_C}\frac{1}{|\mathbf{R}+\boldsymbol{\rho}/2+\mathbf{r}_a-\mathbf{r}_c|}\Bigg\}, \end{aligned} \tag{8}$$

where Z_A, Z_B, and Z_C are the charges of the nuclei of particles A, B, and C in units of the elementary charge e; and N_A, N_B, and N_C are the numbers of electrons in particles A, B, and C. Substituting (8) into the expression for the scattering amplitude derived from (6),

$$M_{\alpha_f\beta_r}(\mathbf{q},\boldsymbol{\rho}) = \int\int \Psi_f^* U e^{-i\mathbf{q}\mathbf{R}}\Psi_i d\mathbf{R}\, d\tau, \tag{9}$$

and integrating over $d^3\mathbf{R}$ via the Bethe integral, we get

$$\begin{aligned} M_{\alpha_f\beta_f}(\mathbf{q},\boldsymbol{\rho}) = \frac{4\pi^2}{q^2}F^A_{\alpha_f\alpha_i}(\mathbf{q}) \Bigg\{ & [F^B_{\beta_f\beta_i}(\mathbf{q},\boldsymbol{\rho}) \\ & + F^C_{\beta_f\beta_i}(\mathbf{q},\boldsymbol{\rho})]\cos\frac{\mathbf{q}\boldsymbol{\rho}}{2} + i[F^B_{\beta_f\beta_i}(\mathbf{q},\boldsymbol{\rho}) \\ & - F^C_{\beta_f\beta_i}(\mathbf{q},\boldsymbol{\rho})]\sin\frac{\mathbf{q}\boldsymbol{\rho}}{2}\Bigg\}, \end{aligned} \tag{10}$$

where $F^A_{\alpha_f\alpha_i}(\mathbf{q})$ is the form factor of particle A,[8] and

$$\begin{aligned} F^B_{\beta_f\beta_i}(\mathbf{q},\boldsymbol{\rho}) = \int \psi^*_{\beta_f}(\mathbf{r}_b,\mathbf{r}_c)\Bigg(& Z_B - \sum_{b=1}^{N_B} \\ & \times e^{-i\mathbf{q}\mathbf{r}_b}\Bigg)\psi_{\beta_i}(\mathbf{r}_b,\mathbf{r}_c)\,d\tau_{BC}, \end{aligned} \tag{11}$$

where $d\tau_{BC}$ is an element of the configuration space of the electrons of the BC molecule, and might well be called the form factor of particle B in the BC molecule. The quantity $F^C_{\beta_f\beta_i}$ is defined similarly. Note that the form factor (11) depends on the vector $\boldsymbol{\rho}$, since $\boldsymbol{\rho}$ enters into the expression for the wave functions of the molecule.

Thus, when the incident plane wave describing the incident A particle is scattered by an arbitrary two-center molecule, it creates a complicated interference pattern. The argument $(\mathbf{q}\rho)/2$ of the trigonometric function is similar to the argument in the problem of interference of electromagnetic waves from two coherent sources. Vector $\boldsymbol{\rho}$ acts as the distance between the sources and $q = 2\pi/\lambda$. The interference amplitude is determined by the form factors.

For symmetric molecules (BC=B_2) we have $F^B = F^C$, and Eq. (10) assumes the form

$$M_{\alpha_f\beta_f}(\mathbf{q},\boldsymbol{\rho}) = \frac{8\pi e^2}{q^2}F^A_{\alpha_f\alpha_i}(\mathbf{q})F^B_{\beta_f\beta_i}(\mathbf{q},\boldsymbol{\rho})\cos\frac{(\mathbf{q}\boldsymbol{\rho})}{2}. \tag{12}$$

Meyerhof *et al.*[22] arrived at the same expression for the H_2 molecule.

In studying processes like (1)–(5), one must sum the differential cross sections (6) over all possible final states of the molecular target and then average the result over the directions of vector $\boldsymbol{\rho}$. Substituting (12) into (6) yields

$$\frac{d\sigma_{\alpha_f}(\nu)}{do} = \frac{16M^2e^4}{\hbar^4 q^4}\frac{k_f}{k_i}|F^A_{\alpha_f\alpha_i}(\mathbf{q})|^2 S^B(\mathbf{q}), \tag{13}$$

where the properties of the target are specified entirely by the function

$$S^B(\mathbf{q}) = \frac{1}{4\pi}\int\sum_{\beta_f}|F^B_{\beta_f\beta_i}(\mathbf{q},\boldsymbol{\rho})|^2\cos^2\left(\frac{\mathbf{q}\boldsymbol{\rho}}{2}\right)d\Omega_\rho, \tag{14}$$

with $d\Omega_\rho$ the element of solid angle in the direction of ρ. The quantity $2S^B(\mathbf{q})$ is the square of the effective charge of the B system in the target molecule. This is evident from the fact that in large-angle scattering we can formally let $q\to\infty$, which yields $S^B=Z_B^2/2$ and $|F^A|^2=Z_A^2$. Substituting these values into Eq. (13), we obtain, as expected, the Rutherford formula multiplied by two, which corresponds to large-angle scattering of nuclei A by the two identical nuclei B of the B_2 molecule.

The sum of the $|F^B_{\beta_f\beta_i}|^2$ in Eq. (14) (including integration over the final-states continuum) can be evaluated in closed form in the Born approximation, i.e., by using a sum rule for the final states along with some representation of the average momentum transfer $\bar{q}$ in collisions.[8,23] Lee and Chen[8] point out that conceptually this method works when the energy E of the H^--ions is at least 100 keV, and even lower energies can be used when estimating cross sections. This corresponds to Bohr's criteria[24,25] for the applicability of the Born approximation: $Z_A\leq Z_B$ and $V>2Z_Bv_0$, where V is the velocity of the incident particle, and $v_0=2.19\cdot10^8$cm/s is the velocity of the electron in the first Bohr orbit of the hydrogen atom. The same is true of scattering processes that leave the charge unaltered. If all this is taken into account, Eq. (13) in the laboratory frame of reference assumes the form

$$\frac{d\sigma_{\alpha_f}(\theta)}{d\Omega}=\frac{16a_0^2}{(\bar{q}a_0)^4}\frac{k_f}{k_i}\left(\frac{M_A}{m_e}\right)^2|F^A_{\alpha_f\alpha_i}(\bar{q})|^2S^B(\bar{q}), \tag{15}$$

where a_0 is the Bohr radius, m_e and M_A are the electron mass and the mass of the A particle, and θ is the scattering angle in the laboratory frame. Equation (14) becomes

$$S^B(\bar{q})=\frac{1}{4\pi}\int\langle\psi_{\beta_i}|\left|Z_B-\sum_{b=1}^{N_B}e^{-i\mathbf{q}\mathbf{r}_b}\right|^2|\psi_{\beta_i}\rangle \times\cos^2\left(\frac{(\mathbf{q}\boldsymbol{\rho})}{2}\right)d\Omega_\rho. \tag{16}$$

Thus, the quantity specified by Eq. (16) is determined solely by the wave function of the ground state of the target molecule.

Ordinarily one uses Eq. (13) when calculating total cross sections, substituting $do=\pi d(q^2)/k_fk_i$ for $d\Omega$. We, however, are interested not only in total sections but also in the angular characteristics of processes (1)–(5) in the laboratory frame. Hence the calculations of differential and total cross sections were carried out via Eq. (15).

In the case of an H_2 target, Eq. (16) becomes

$$S^H(\bar{q})=\frac{1}{2\pi}\int F_s^H(\bar{q})\cos^2\frac{(\mathbf{q}\boldsymbol{\rho})}{2}d\Omega_\rho, \tag{17}$$

where $F_s^H(\bar{q})=1-\langle\psi^{H_2}_{\beta_i}|e^{i\mathbf{q}\mathbf{r}}|\psi^{H_2}_{\beta_i}\rangle$ is the form factor (11) for the singlet ground state of the H_2 molecule. Here, for the sake of simplicity, the label on the radius vector $\mathbf{r}$ has been dropped, while the subscript "s" indicating the singlet state of the H_2 molecule in the notation of the form factor distinguishes this form factor from the conventional notation for the hydrogen-atom form factor.

The ground state of the hydrogen molecule is described by the Wang wave function.[26] We call the corresponding function $F_s^H(\bar{q})$ from Eq. (17) the Wang form factor. The expression for the Wang form factor contains the following product of integrals:

$$\int\exp\{-(Z/a_0)(|\mathbf{r}-\boldsymbol{\rho}|+r)\}\exp i(\mathbf{q}\mathbf{r})d\mathbf{r}\int \times\exp\{-(Z/a_0)(|\mathbf{r}'+\boldsymbol{\rho}|+r')\}d\mathbf{r}' \cong\frac{16\pi^2a_0^6S^2}{Z^2(4Z^2+q^2a_0^2)^2}\exp[i(\mathbf{q}\boldsymbol{\rho})/2], \tag{18}$$

which was approximated, as in Ref. 22, by the right-hand side of Eq. (18). For the Wang wave function, $Z=1.166$, $\rho=0.76$Å, and the overlap integral $S=(1+x+x^2/3)e^{-x}=0.67633$, with $x=Z\rho/a_0$. Using (18), we arrive at the following form of Eq. (17):

$$S^H(\bar{q})=1-\frac{3}{2}Q+\frac{1}{\gamma}\left\{(1-2Q)\sin\gamma-\frac{Q}{4}\sin2\gamma -6QS^2\left[\sin\frac{\gamma}{2}+\frac{1}{9}\sin\frac{3\gamma}{2}\right]\right\}, \tag{19}$$

where $\gamma=\bar{q}\rho$, and the Wang form factor is

$$Q=\frac{8Z^4}{(1+S^2)(4Z^2+\bar{q}^2a_0^2)^2}.$$

Note that the approximation (18) leads to the correct functional dependence of (19) on $\bar{q}$ for small $\bar{q}$, i.e., for scattering angles close to zero. In particular, at $\bar{q}=0$, the expression (16) obviously vanishes if $Z_B=N_B$; the same follows from (19).

In addition to the function (19) obtained here, to calculate the cross sections of processes (1)–(5) we used the square of the effective charge S_s+S_a found by Meyerhof *et al.*[22] via the Weinbaum wave function for the H_2 molecule. The sum S_s+S_a from Ref. 22 is related, by definition, to the function (19): $S_s+S_a=4S^H(\bar{q})$. Using the more complicated Weinbaum wave function leads only to a slight change in the constants that enter into the definition of Q, and in the factor $6S^2$. In the same paper Meyerhof *et al.* calculated S_s+S_a using the Stewart form factor. We also used their result in calculating the cross sections of processes (1)–(5). The expressions for the functions $S^H(\bar{q})$ from (17) or S_s+S_a corresponding to the Weinbaum and Stewart form factors can easily be derived from Ref. 22, and we will not write them out here. The expressions for the form factors of the incident particles and the incoherent scattering functions $S^H_{inc}(\bar{q})$ for H^- ions, which are needed to calculate the cross sections of processes (1)–(5), can be found in Ref. 11. Below we compare the characteristic angles and cross sections obtained via the Wang, Weinbaum, and Stewart form factors with the existing experimental and theoretical results.

4. DISCUSSION

We have calculated angles[11,19] and total scattering cross sections for hydrogen particles with energies $E=0.1$–20 MeV in a H_2 target using Eq. (15) for the three form factors

mentioned above. For the process specified by (3), the scattering of H^- ions leaving charge unaltered, the final state of the H^- ion is the ground state because the excited states are autodetached.[1] Applying the sum rule to $|F^{H^-}_{\alpha_f}|^2$ in (15) for $\alpha_f \neq \alpha_i$ yields the differential scattering cross section for the superposition $(\bar{1}0)+(\bar{1}1)$ of processes (4) and (5), i.e., the cross sections

$$\frac{d\sigma_\Sigma}{d\Omega}=\frac{d\sigma_{\bar{1}0}}{d\Omega}+\frac{d\sigma_{\bar{1}1}}{d\Omega}$$

and

$$\sigma_\Sigma=\sigma_{\bar{1}0}+\sigma_{\bar{1}1}$$

along with the characteristic angles $\theta^\Sigma_{1/2}\equiv\theta^{(\bar{1}0)+(\bar{1}1)}_{1/2}$. However, $\sigma_{\bar{1}1}$ is only four-hundredths of $\sigma_{\bar{1}0}$ (see Refs. 1, 2 and Table I). This makes it possible to estimate quite accurately the characteristic angles and cross sections for neutralization of the H^- ions. Computed results are listed in Tables II–IV, where we have introduced the notation $\sigma_{00}=\sigma_{00}(1s)+\sigma_{00}(2s)+\sigma_{00}(2p_0)$. Table IV lists the parameters contained in the asymptotic expressions for the characteristic angles and cross sections as functions of energy:

$$\theta^\Sigma_{1/2},\theta^{(00)}_{1/2}=\frac{k_{ij}}{E^{1/2}},\quad \theta^{(\bar{1}\bar{1})}_{1/2}=\frac{k_{\bar{1}\bar{1}}}{E},\quad \theta^{(11)}_{1/2}=\frac{k_{11}}{E}, \tag{20}$$

$$\sigma_\Sigma,\sigma_{00}=\frac{c_{ij}}{E},\quad \sigma_{\bar{1}\bar{1}}=\frac{c_{\bar{1}\bar{1}}}{E},\quad \sigma_{11}=c_{11}\frac{\ln(E/a)}{E}. \tag{21}$$

The parameters have numerical values such that when substituted into Eqs. (20) and (21) they yield angles in units of μrad and cross sections in units of 10^{-18}cm^2 if E is measured in MeV. The values of $\sigma_{00}(1s)$ and σ_{11} are not listed in Table II because they can be determined from Eqs. (21) to full accuracy over the entire 0.1–20 MeV energy range.

Analysis of the results of calculations for the H_2 target produced the following results:

1. The differential scattering cross sections for the processes (1)–(5) have the same shape and features as in scattering from H and He targets.[11,12]

2. All form factors employed yield essentially the same values of the characteristic scattering angles (except the angle $\theta^{(00)}_{1/2}$ for $E=0.1$–1 MeV), close to those calculated in Ref. 12 for an atomic hydrogen target, especially for $E>1$MeV. Experimental data on the characteristic scattering angles for a H_2 target exist only for the $(\bar{1}0)$ process and $E=50$–150 keV (Ref. 17); the calculated values of the angles $\theta^\Sigma_{1/2}$ are approximately 1.3 times smaller than the $\theta^{(\bar{1}0)}_{1/2}$ measured by Dyachkov *et al.*;[17] over this energy range, however, they obey a $\theta^\Sigma_{1/2}\sim E^{-0.67}$ law rather than a $\theta^{(10)}_{1/2}\sim E^{-0.5}$ law.

3. For the angles $\theta^{(\bar{1}\bar{1})}_{1/2}$ and $\theta^{(11)}_{1/2}$, the Weinbaum form factor over the range $E=5$–20 MeV leads to angles that vary much more rapidly than E^{-1} (the functions do not reach their asymptotic limit), which is probably incorrect. Therefore, the corresponding coefficients $k_{\bar{1}\bar{1}}$ and k_{11} listed in Table IV only approximate the energy dependence and do not characterize asymptotic behavior.

4. The cross sections obtained with the Wang and Weinbaum form factors differ only by 5% at all values of E, while the cross sections calculated with the Stewart form factor are smaller than the above cross sections by a factor 1.5–2.5. For

TABLE II. Total cross sections (in units of 10^{-18}cm^2) for the scattering of hydrogen particles in a H_2 target with electron detachment and with no alteration of charge, calculated in the present work.

E, MeV	σ_Σ	σ_{00}	$\sigma_{00}(2s)$	$\sigma_{00}(2p)$	$\sigma_{\bar{1}\bar{1}}$
	1287	186.0	11.63	39.18	207.6
0.1	1248	182.3	11.27	37.75	202.1
	669.2	124.8	5.54	17.00	128.5
	911.3	130.2	8.22	31.74	184.7
0.15	882.6	127.4	7.95	30.54	179.0
	466.2	85.60	3.87	13.51	103.2
	705.8	100.3	6.31	26.30	168.9
0.2	688.3	98.1	6.11	25.28	163.3
	358.0	65.21	2.96	11.09	88.84
	486.8	68.82	4.29	19.39	145.9
0.3	471.1	67.27	4.15	18.63	140.7
	244.8	44.21	2.00	8.10	71.73
	371.6	52.40	3.24	15.29	129.2
0.4	359.6	51.20	3.13	14.69	124.6
	136.1	33.46	1.51	6.36	61.23
	214.4	30.14	1.84	9.20	97.26
0.71	207.4	29.44	1.78	8.84	93.79
	106.7	19.08	0.857	3.81	43.67
	153.6	21.57	1.305	6.70	80.14
1.0	148.6	21.07	1.263	6.43	77.37
	76.30	13.62	0.609	2.76	35.16
	92.77	13.02	0.781	4.11	58.31
1.67	89.78	12.71	0.755	3.95	56.47
	46.00	8.19	0.364	1.69	24.92
	51.94	7.28	0.434	2.325	39.21
3.0	50.27	7.11	0.420	2.233	38.22
	25.72	4.58	0.203	0.956	16.40
	31.26	4.38	0.261	1.407	27.12
5.0	30.26	4.28	0.252	1.352	26.69
	15.47	2.75	0.121	0.578	11.18
	22.69	3.18	0.189	1.024	21.31
6.9	21.96	3.10	0.183	0.984	21.15
	11.22	1.944	0.0880	0.420	8.723
	15.07	2.11	0.125	0.682	15.55
10.4	14.60	2.06	0.121	0.655	15.66
	7.45	1.323	0.0584	0.280	6.313
	10.53	1.474	0.0875	0.477	11.71
14.9	10.20	1.440	0.0847	0.459	12.01
	5.20	0.924	0.0408	0.196	4.729
	7.85	1.099	0.0653	0.356	9.26
20.0	7.60	1.073	0.0631	0.342	9.67
	3.88	0.6883	0.0304	0.146	3.720

For each value of the collision energy E we list three values of the cross sections corresponding (successively downward) to calculations done with the Wang, Weinbaum, and Stewart form factors.

TABLE III. Characteristic scattering angles (in units of 10^{-6}rad) for fast hydrogen particles in an H_2 target with electron detachment and with no alteration of charge, calculated in the present work.

E, MeV	$\theta_{1/2}^{\Sigma}$	$\theta_{1/2}^{(00)}$	$\theta_{1/2}^{(\bar{1}\bar{1})}$	$\theta_{1/2}^{(11)}$
	112.0	197.0	43.2	71.8
0.1	113.0	200.0	43.2	71.9
	120.0	334.0	43.5	73.8
	86.1	143.0	32.0	48.9
0.15	86.4	144.0	32.0	48.9
	91.3	225.0	32.2	49.9
	72.1	117.0	25.7	37.1
0.2	72.3	119.0	25.7	37.1
	76.2	147.0	25.8	37.7
	56.8	91.7	18.6	25.0
0.3	56.9	92.6	18.6	25.0
	59.7	108.0	18.7	25.3
	48.2	77.8	14.7	18.9
0.4	48.4	78.5	14.7	18.8
	50.7	90.3	14.8	19.1
	35.3	56.9	9.05	10.7
0.71	35.4	57.4	8.99	10.7
	37.0	65.0	9.07	10.8
	29.5	47.5	6.69	7.65
1.0	29.5	47.9	6.63	7.56
	30.8	54.0	6.71	7.68
	22.6	36.5	4.20	4.60
1.67	22.6	36.8	4.13	4.51
	23.6	41.2	4.21	4.61
	16.7	27.1	2.43	2.57
3.0	16.7	27.3	2.35	2.48
	17.5	30.5	2.43	2.57
	12.9	20.9	1.49	1.54
5.0	12.9	21.1	1.41	1.45
	13.5	23.5	1.49	1.54
	11.0	17.8	1.09	1.12
6.9	11.0	17.9	1.01	1.03
	11.5	20.0	1.09	1.12
	8.93	14.5	0.729	0.742
10.4	8.94	14.6	0.653	0.662
	9.32	16.2	0.729	0.742
	7.46	12.1	0.511	0.518
14.9	7.46	12.2	0.441	0.445
	7.78	13.6	0.512	0.518
	6.43	10.4	0.382	0.386
20.0	6.44	10.5	0.317	0.319
	6.71	11.7	0.382	0.386

For each value of the collision energy E we list three values of the angles corresponding (successively downward) to calculations done with the Wang, Weinbaum, and Stewart form factors.

TABLE IV. Parameters used in the asymptotic formulas (20) and (21) for the characteristic angles and the cross sections of the processes $(\bar{1}0)+(\bar{1}1)$, (00), $(\bar{1}\bar{1})$, and (11) calculated for an H_2 target via the Wang form factor and the Weinbaum and Stewart form factors taken from Ref. 21.

		Form factors		
Process	Parameter	Wang	Weinbaum	Stewart
$(\bar{1}0)+(\bar{1}1)$	k_{Σ}	28.6	28.80	30.01
	c_{Σ}	157.0	152.0	77.60
(00)	k_{00}	46.5	46.6	52.3
	c_{00}	21.98	21.46	13.77
	$c_{00}(1s)$	13.55	13.35	10.24
	$c_{00}(2s)$	1.306	1.262	0.608
	$c_{00}(2p)$	7.12	6.84	2.92
$(\bar{1}\bar{1})$	$k_{\bar{1}\bar{1}}$	7.64	6.63^{ap}	7.64
	$c_{\bar{1}\bar{1}}$	90.2	83.6	35.16
	n	0.76	0.72	0.75
(11)	k_{11}	7.72	7.56^{ap}	7.72
	c_{11}	36.05	39.82	13.46
	a	5906	11 360	2663

The quantity a is given in units of 10^{-6} MeV. The superscript "ap" on the coefficients k_{ff} and k_{11} obtained with the Weinbaum form factor indicates that the coefficients approximate the E dependence of $\theta_{1/2}^{(\bar{1}\bar{1})}$ and $\theta_{1/2}^{(11)}$, and do not reflect the asymptotic behavior, which in the 5–20 MeV energy range is not even achieved.

the $(\bar{1}0)+(\bar{1}1)$ process, they are in good agreement with our experimental data and the data of other researchers, as well as with the results of theoretical calculations[8] (see Fig. 3).

5. The cross sections σ_{11}, σ_{00}, and $\sigma_{\bar{1}\bar{1}}$ calculated with the Stewart form factor in the present paper coincide, if the experimental error is taken into account, with the measured cross sections of Refs. 11 and 18.

6. The relations between the constant-charge cross sections and the ratio of these cross sections to σ_{Σ} was found to be approximately the same as for an atomic hydrogen target.[12]

7. Comparison of the characteristic angles and cross sections of processes (2)–(5) for an H_2 target with the same specifications as a He target, similar to the comparison in Ref. 12, points up the utility of using H_2 targets to obtain strong low-emittance beams of hydrogen atoms by neutralizing H^- ions.

As for our experimental cross sections σ_{01} for the H_2 target, these proved to be 30% greater than the values calculated by Riesselmann *et al.*[9] and agreed, to within the experimental errors, with the values of σ_{01} calculated by Meyerhof *et al.*[22] with the Stewart form factor.

In the case of a helium target, our experimental data (Table I) for the sum of processes, $(\bar{1}0)+(\bar{1}1)$, coincide to within the experimental errors with the results of calculations in Refs. 6, 8 and 11, and are in good agreement with the results of experiments done by Smythe and Toevs[15] and Dimov and Dudnikov.[16] On the average, the cross sections σ_{01}(He) are 30% above those calculated by Riesselmann *et al.*[9] The cross sections σ_{01} for the O_2 target obtained in the present work are essentially identical with those obtained by Berkner, Kaplan, and Pyle.[9]

Systematic experimental data on the cross sections σ_{01}, $\sigma_{\bar{1}0}$, and $\sigma_{\bar{1}1}$ for $E>1$MeV pertaining to targets comprised of heavier gases exist only for argon[10,14,15,27,28] and agree with our cross section listed in Table I to within the experimental errors. Comparison of the cross sections σ_{01} and $\sigma_{\bar{1}0}$ calculated by Riesselmann *et al.*[9] and measured in the present work for Ar, Kr, and Xe targets shows that the

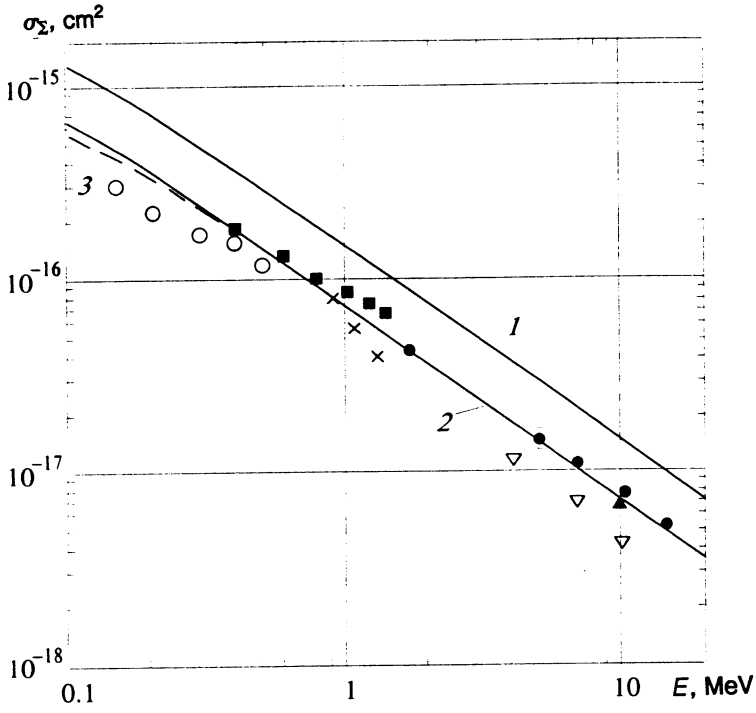

FIG. 3. Cross sections σ_Σ of electron losses by the H^- ions in a H_2 target. Theoretical results (solid and dashed curves): curve *1*, the cross sections calculated in the present work with the Wang and Weinbaum form factors (which are essentially identical on the scale of the figure); curve *2*, the cross section calculated in the present work with the Stewart form factor; and curve *3*, the cross section calculated in Ref. 9 (for $E>0.5$ MeV this curve coincides with curve *2*). Experimental data: ● results of the present work; △—Ref. 5; ○—Ref. 13; ■—Ref. 14; ▲—Ref. 15; ×—Ref. 16. The results of studies from Ref. 14 and 16 for $E=1.3$ MeV given in this figure correspond to $\sigma_{\bar{1}0}$ section.

theoretical curves for the cross sections fall, as the energy increases, somewhat faster than the experimental curves, intersecting the latter near $E=10$ MeV.

Table I demonstrates that all the cross sections of electron loss by fast hydrogen particles that we measured follow an approximate power-law energy dependence, $\propto E^{-n}$. Here the spectral index $n\cong 1$ for He and H_2, and decreases as the target's atomic number rises. This is probably due to a relative rise in the probability of occurrence of the processes studied here with increasing energy E, provided that the relative velocity of the colliding particles approaches in magnitude the average orbital velocity of the electrons in the inner shells of the target atoms.

Comparing the electron-loss cross section $\sigma_{\bar{1}0}$ and σ_{01} (Table I) with the constant-charge hydrogen-particle cross sections σ_{ii} (Ref. 11) at $E=1.67$ MeV, we see that for all targets the cross sections in question are of similar magnitude, and that $\sigma_{00}/\sigma_{\bar{1}0}=0.17-0.40$, $\sigma_{00}/\sigma_{01}=0.63-0.95$, $\sigma_{\bar{1}\bar{1}}/\sigma_{\bar{1}0}=0.25-0.56$, and $\sigma_{11}/\sigma_{01}=2.4-4.0$. From the viewpoint of formation of beams of H^0 and H^+ particles with minimal angular divergence by stripping H^- ions, these relations are such (all other things being equal) that a H_2 target proves to be the best for forming a beam of H^0 atoms and the worst for forming a proton beam. Note that in choosing a target it is important to thoroughly study and compare not only the cross sections, but also the angular characteristics of fast hydrogen-particle scattering processes with and without charge alteration.

5. CONCLUSION

1. The electron-loss cross sections found in our experiments coincide, to within the measurement errors, with the existing experimental and theoretical data for H_2, He, and Ar targets, which suggests that the data on cross sections obtained for other gases are accurate.

2. Calculations carried out in the present work for an H_2 target with the Stewart form factor yield cross sections σ_Σ, $\sigma_{\bar{1}\bar{1}}$, σ_{00}, and σ_{11} that agree in the best possible way with the existing experimental and theoretical results. The characteristic angles exhibit the correct energy dependence,[7,8,11,12,17] and usually only slightly exceed the corresponding angles calculated on the basis of the Wang and Weinbaum form factors over the entire 0.1–20 MeV energy range. Bearing all this in mind, let us examine the problem of errors in calculating the total cross sections of the processes (1)–(5). By the error of a calculated quantity we mean the probable deviation of that quantity from its true value, which, in the absence of other criteria, is established empirically. Then the computational error is determined by the measurement error in the quantity with which the comparison is made. The fact that the theoretical results coincide with the experimental data (to within the measurement errors) at points in the method's range of applicability generally makes it possible to assess, with a certain degree of accuracy, the validity of the calculations over the method's full range of applicability. For instance, in the computational model that we used with the Stewart form factor for all $E\geqslant 0.7$ MeV, the error in calculating the cross section σ_Σ amounted to 10%, while for the other cross sections the error was 25%. Near the lower boundary of the range within which the Born approximation could be applied, $E\simeq 100$ keV, the given computational model probably overestimates values (by approximately a factor 1.5 for $E=100-150$ keV) of the cross sections in comparison to the measured values (see Fig. 3 and Ref. 8), i.e., the theoretical

approach carries a systematic error. At the same time, the choice of wave functions for the description of colliding particles may have a significant effect on the computational error. For instance, using the Wang and Weinbaum wave functions for the H_2 target, we found cross sections for the processes (1)–(5)that are approximately twice the cross section calculated with the Stewart form factor, while using different wave functions for the H^- ion changes the calculated values of the cross sections by only 5–10% (cf. Ref. 8 and Refs. 11 and 12).

3. It is known[8,11,12] that the characteristic angles $\theta_{1/2}^{\bar{1}\bar{1}}$ and $\theta_{1/2}^{(11)}$ are comparable in magnitude with the angles $\theta_{1/2}^{(\bar{1}0)}$ and $\theta_{1/2}^{(01)}$, but that $\theta_{1/2}^{(00)} \gg \theta_{1/2}^{(\bar{1}0)}$. The result is that in some technical applications, when a beam of particles with low angular divergence is formed, a fraction of particles scattered with unaltered charge through large angles must be considered lost to further utilization. Naturally, this fraction grows with target thickness and, starting at a certain t, even faster than the beam fraction with the required charge. Hence for each specific case, the optimum target thickness t^{opt} should be selected. Obviously, in preparing a beam of hydrogen atoms with low emittance via the neutralization of H^- ions, the value of t^{opt} will be somewhat lower than $t^{\max}$, with $\Phi_0^{\text{opt}} < \Phi_0^{\max}$.

4. Bearing in mind the essence of the applied problems noted in the Introduction and the analysis of the results of the present work, we can conclude that it would be worthwhile to study the total cross sections and angular characteristics of electron-loss processes $(\bar{1}0)$, $(\bar{1}1)$, and (01), scattering processes $(\bar{1}\bar{1})$, (00), and (11) with no charge alteration, and $(\bar{1}0)$ processes with formation of hydrogen atoms in excited nl-states for a broad spectrum of targets and energy ranges.

The authors would like to note the role of the late P. A. Demirkhanov and the late D. V. Chkuaseli in the statement of the experimental problem. The authors are also deeply grateful to V. N. Kudryavtsev and Yu. G. Lazarev and many others for the help in preparing and carrying out the measurements.

[1] H. S. Massey, *Negative Ions*, 3rd ed., Cambridge Univ. Press, Cambridge (1976).
[2] N. V. Fedorenko, Zh. Tekh. Fiz. **40**, 2481 (1970) [Sov. Phys. Tech. Phys. **15**, 1947 (1971)].
[3] J. S. Risley, in *Electronic and Atomic Collisions. Invited Papers and Progress Reports* (Proc. 11th Int. Conf., Kyoto, 29 August–4 September, 1979), N. Oda and K. Takayanagi (eds.), North-Holland, Amsterdam (1980), p. 619.
[4] H. Tawara and A. Russek, p **45**, 178 (1973).
[5] D. P. Dewangan and H. R. J. Walters, J. Phys. B **11**, 3983 (1978).
[6] G. H. Gillespie, Phys. Rev. A **15**, 563 (1977).
[7] J. A. Johnstone, NIM Phys. Res. B **52**, 1 (1990).
[8] Y. T. Lee and J. C. Y. Chen, Phys. Rev. A **19**, 526 (1979).
[9] K. Riesselmann, L. W. Anderson, L. Durand, and C. J. Anderson, Phys. Rev. A **43**, 5934 (1991).
[10] K. H. Berkner, S. N. Kaplan, and R. V. Pyle, Phys. Rev. **134**, A1461 (1964).
[11] V. I. Radchenko, Zh. Eksp. Teor. Fiz. **103**, 40 (1993) [JETP **76**, 229 (1993)].
[12] V. I. Radchenko, Zh. Eksp. Teor. Fiz. **105**, 834 (1994) [JETP **78**, 445 (1994)].
[13] J. Heinemeier, P. Hvelplund, and F. R. Simpson, J. Phys. B **9**, 2679 (1976).
[14] P. H. Rose, R. J. Connor, and R. P. Bastide, Bull. Amer. Phys. Soc. **3**, 40 (1958).
[15] R. Smythe and J. W. Toevs, Phys. Rev. **139**, A15 (1965).
[16] G. I. Dimov and V. G. Dudnikov, Zh. Tekh. Fiz. **36**, 1239 (1966) [Sov. Phys. Tech. Phys. **11**, 919 (1966)].
[17] B. A. Dyachkov, V. I. Zinenko, and G. V. Kazantsev, Zh. Tekh. Fiz. **47**, 416 (1977) [Sov. Phys. Tech. Phys. **22**, 245 (1977)].
[18] V. I. Radchenko, Zh. Tekh. Fiz. **63**, 200 (1993) [Tech. Phys. **38**, 260 (1993)].
[19] V. I. Radchenko, Zh. Tekh. Fiz. **62**, 132 (1992) [Sov. Phys. Tech. Phys. **37**, 431 (1992)].
[20] G. D. Ved'manov, V. P. Kozlov, V. N. Kudryavtsev *et al.*, Prib. Tekh. Eksp. **2**, 47 (1989).
[21] L. D. Landau and E. M. Lifshitz, *Quantum Mechanics: Nonrelativistic Theory*, 3rd ed., Pergamon Press, Oxford (1977).
[22] W. E. Meyerhof, H.-P. Hulskotter, Qiang Dai *et al.*, Phys. Rev. A **43**, 5907 (1991).
[23] M. Inokuti, p **43**, 297 (1991).
[24] N. Bohr, *The Penetration of Atomic Particles through Matter*, Kgl. Danske Videnskab. Selskab. Mat.-Fys. Medd. **18**, 8 (1948).
[25] I. S. Dmitriev, Ya. M. Zhileıkin, and V. S. Nikolaev, Zh. Eksp. Teor. Fiz. **49**, 500 (1965) [Sov. Phys. JETP **22**, 352 (1966)].
[26] A. S. Davydov, *Quantum Mechanics*, 2nd ed., Pergamon Press, Oxford (1976).
[27] L. M. Welsh, K. H. Berkner, S. N. Kaplan, and R. V. Pyle, Phys. Rev. **158**, 85 (1967).
[28] L. N. Toburen, M. Y. Nąkai, and R. A. Langley, Phys. Rev. **171**, 114 (1968).

Translated by Eugene Yankovsky